TISSUE ENGINEERING
Volume 11, Number 7/8, 2005

Assessment of Tissue Ingrowth Rates in Polyurethane Scaffolds for Tissue Engineering

NAVIN N. RAMRATTAN, M.D.,[1] RALF G.J.C. HEIJKANTS, Ph.D.,[2] TONY G. VAN TIENEN, M.D., Ph.D.,[1] AREND JAN SCHOUTEN, Ph.D.,[2] RENE P.H. VETH, M.D., Ph.D.,[1] and PIETER BUMA, Ph.D.[1]

ABSTRACT

The continuous development of new biomaterials for tissue engineering and the enhancement of tissue ingrowth into existing scaffolds, using growth factors, create the necessity for developing adequate tools to assess tissue ingrowth rates into porous biomaterials. Current histomorphometric techniques evaluating rates of tissue ingrowth tend either to measure the overall tissue content in an entire sample or to depend on the user to indicate a front of tissue ingrowth. Neither method is particularly suitable for the assessment of tissue ingrowth rates, as these methods either lack the sensitivity required or are problematic when there is a tissue ingrowth gradient rather than an obvious tissue ingrowth front. This study describes a histomorphometric method that requires little observer input, is sensitive, and renders detailed information for the assessment of tissue ingrowth rates into porous biomaterials. This is achieved by examining a number of computer-defined concentric zones, which are based on the distance of a pixel from the scaffold edge. Each zone is automatically analyzed for tissue content, eliminating the need for user definition of a tissue ingrowth front and thus reducing errors and observer dependence. Tissue ingrowth rates in two biodegradable polyurethane scaffolds (Estane and polycaprolactone–polyurethane [PCLPU]) specifically designed for tissue engineering of the knee meniscus were assessed. Samples were subcutaneously implanted in rats with follow-up until 6 months. Especially at the earlier follow-up points, PCLPU scaffolds showed significantly higher tissue ingrowth rates than Estane scaffolds, making the PCLPU scaffold a promising candidate for further studies investigating meniscus tissue engineering.

INTRODUCTION

TISSUE ENGINEERING is a multidisciplinary field of biomedical research that merges the fields of cellular and molecular biology, cell and tissue culture techniques, and materials sciences to recreate tissue for treatments involving reconstruction or replacement. New biocompatible materials are developed constantly for use as scaffolds in tissue engineering of a wide variety of tissues and structures such as cartilage, bone, liver, blood vessels, heart valves, and the knee meniscus.[1–19] In general, however, depending on the tissue that is to be engineered, two main tissue-engineering approaches can be distinguished.

In the first and currently the most popular approach, cells are seeded onto scaffolds and cultured *in vitro* to form a construct that subsequently is implanted into a laboratory animal. Here the construct can further mature and/or start functioning immediately. Although successful in some cases (i.e., heart valves[20]), the main disad-

[1]Orthopedic Research Laboratory, University Medical Center Nijmegen, Nijmegen, The Netherlands.
[2]Department of Polymer Chemistry, University of Groningen, Groningen, The Netherlands.

vantage of this approach is that cells in the tissue-engineered construct must deal with a relative lack of nutrients *in vivo* in the early posttransplantation period, as compared with the ideal circumstances they were accustomed to *in vitro*. This dearth of resources may result in cell death and ultimately lead to failure of the entire tissue engineering construct.[21–23]

In the alternative approach that is gaining popularity, especially with the advent of so-called smart scaffolds,[24–26] acellular scaffolds are implanted into a laboratory animal. Rather than relying on *in vitro* seeding of cells as in the first approach, this alternative approach relies on *in vivo* ingrowth of surrounding tissue into the scaffold with subsequent proliferation and differentiation into the desired tissue. Especially in large three-dimensional (3D) scaffolds, with a size exceeding the critical diffusion distance, this approach will be useful when ingrowth of vascularized tissue can be induced.[25]

The development of new biomaterials for tissue engineering, and the enhancement of tissue ingrowth into existing materials by means of attaching growth factors ("smart scaffolds"), create the necessity to develop tools for assessment of tissue ingrowth rates into porous biomaterials. With the advent of sophisticated image analysis software and desktop processing power, for most groups histomorphometry will be the most affordable and versatile tool for this purpose.

Current histomorphometric techniques to assess rates of tissue ingrowth into a scaffold tend to depend on either a user-defined tissue ingrowth front[27] or an overall measurement of the tissue content in an entire sample.[28] Neither method is particularly suited for assessment of the rate of tissue ingrowth. A clear tissue ingrowth front is often difficult to define or even absent, making user intervention necessary, which is not only time consuming but also inevitably introduces errors. Overall measurement of the tissue content in the entire sample is less time consuming but can be too crude a method to detect small differences in tissue ingrowth rates, especially in large samples or when follow-up intervals are short.

This study investigates tissue ingrowth rates into a newly developed polycaprolactone–polyurethane scaffold (PCLPU) and an existing Estane scaffold currently being studied by the authors for use in meniscus tissue engineering.[18] On degradation *in vivo*, Estane scaffolds are thought to release potentially toxic and carcinogenic metabolites, such as methylenedianiline[29] that may prevent clinical application of such scaffolds in patients. A histomorphometric analysis was performed on scaffold samples that had been implanted subcutaneously in rats with follow-up times of up to 6 months. If the nontoxic PCLPU scaffold[30,31] allows sufficient tissue ingrowth, it provides a promising alternative to Estane for further animal and clinical studies investigating biodegradable scaffolds for use in meniscus tissue engineering.

We aimed to determine whether the extent and rate of tissue ingrowth in PCLPU scaffolds differ from those in Estane scaffolds. In addition, we aimed to demonstrate the application of a histomorphometric method that is sensitive and fast, and that renders detailed information for the assessment of tissue ingrowth rates while requiring minimal observer input.

MATERIALS AND METHODS

Polymers

Estane 5701-F1 implants (BF Goodrich Chemical, Westerlo-Oevel, Belgium) consisted of a 4,4-methylenediphenyldiisocyanate-based hard segment and a soft segment of adipic acid and butane diol. Estane was dissolved in 1,4-dioxane at 80°C (35%, w/w) and water (8% [w/w] relative to dioxane) was added as a nonsolvent. The polymer solution was mixed with saccharose crystals (150–350 μm) and cooled −18°C. After freezing, the solvent was removed by freeze-drying and subsequently the saccharose was dissolved in water to create pores.[32]

The PCLPU scaffolds consisted of a hard segment of 1,4-butanediisocyanate and butane diol and a soft segment of poly(ϵ-caprolactone) and were synthesized as described elsewhere.[33] Pores in the PCLPU scaffolds were created by adding sodium chloride crystals (150–355 μm) that were washed out afterward.[33] All pores were interconnected to achieve high permeability of the polymer. Porosity was 78%. The compression modulus of both implants at 20% strain was 300 kPa. Both PCLPU and Estane scaffold samples were manually cut into cubes of $7 \times 7 \times 7$ mm.

Surgery

Twenty-four male Wistar rats between 200 and 250 g underwent surgery while anesthetized with nitrous oxide (1:1) and isoflurane (0.5%). After shaving and disinfecting the skin, two skin incisions were made in the back of each rat. A narrow, subcutaneous tunnel was created toward each upper extremity of the rat by mobilizing the skin from the underlying fascia. One sample of a scaffold material was placed at the end of a tunnel, roughly over the scapula. Each rat received two scaffold samples, one of each material. The dorsal skin incision was closed with three staple clips.

The Wistar rats were housed under standard GLP conditions, with an adequate supply of food and water. The institutional animal welfare committee approved all procedures.

One, 4, 8, and 26 weeks postimplantation, six rats were killed with a lethal dose of nitrous oxide (1:1) and isoflurane (0.5%), after which scaffold samples were carefully harvested from the subcutaneous compartment.

Histology

Scaffold samples were fixed in acetone (−20°C) for 6 h, infiltrated in methylmethacrylate, and polymerized at −20°C for 2 days. Sections (7 μm thick) were cut from the middle of each sample. This way the center of a section corresponds with the center of a 7 × 7 × 7 mm scaffold cube. As samples were found to rotate quite easily in the loose connective tissue of the subcutaneous compartment, it was unlikely that the spatial orientation of the midsections (regarding the *x*, *y*, or *z* axis) was of much influence on ingrowth. Sections were dried at 37°C, deacrylated in warm xylol, and stained. In each section, Sudan black was used to stain the polymer blue and nuclear fast red was used to stain the ingrown tissue red; this includes the cell body and the extracellular matrix deposited by these cells. Unfilled pores obviously remained unstained. All samples were stained according to the same protocol and in a limited number of batches, ensuring a highly homogeneous staining intensity for all samples.

Three sections of each sample were microscopically assessed (magnification, ×40) (Axioplan 2 microscope; Carl Zeiss, Thornwood, NY) to determine the nature of the ingrown tissue and to determine the presence of a foreign body reaction (i.e., presence of macrophages, giant cells, and polymorphonuclear leukocytes).

Histomorphometry

Sections were digitized at a magnification of ×25 and a resolution of 1600 × 1200 pixels, using a Camedia C-

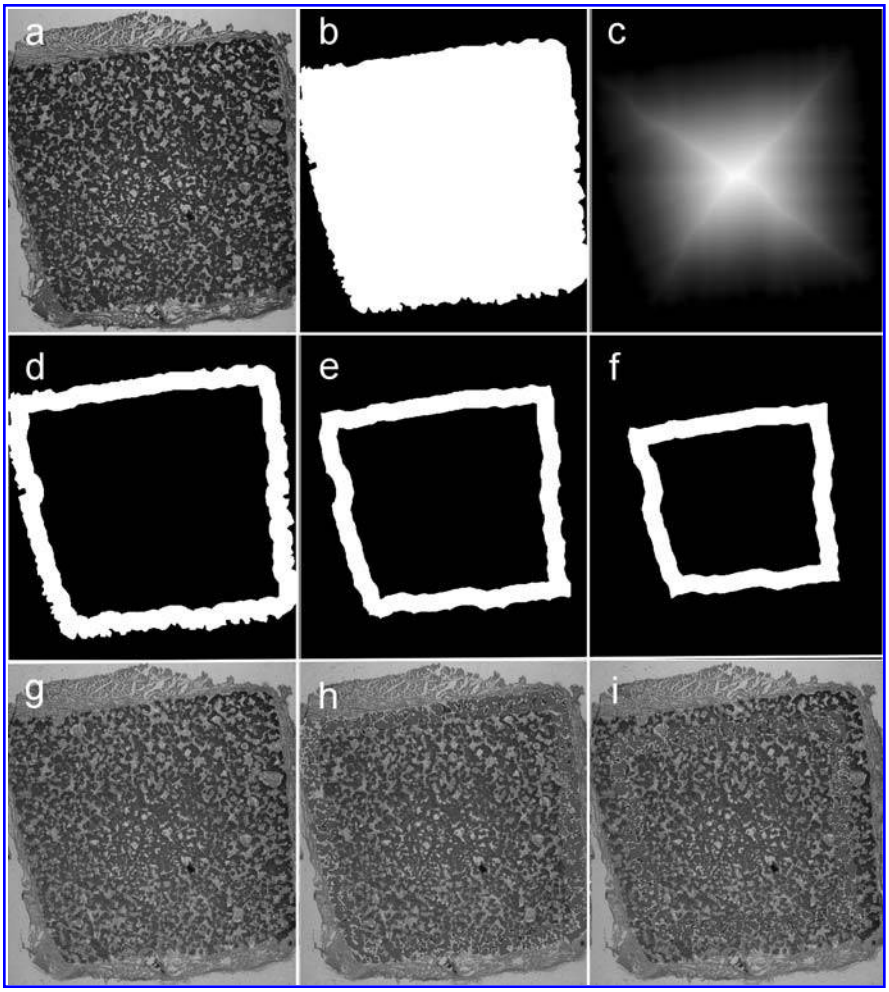

FIG. 1. (**a**)Original digitized image that is outlined by the observer. (**b**) The outline is converted to a binary mask. (**c**) Grayscale euclidian distance map based on binary mask. Pixels are lighter the farther away their location is from the edge. (**d–f**) Seven threshold ranges are applied to the distance map to create seven binary masks representing the zones (only three are shown here: zone 1, zone 2, and zone 3). (**g**) Colors in the original image are adjusted in the hue–saturation–intensity range to create optimal contrast between tissue (green) and scaffold (red). (**h** and **i**) False color coding indicating each zone being measured separately, using the binary masks shown under (**d**) and (**e**).

4040 digital camera (Olympus America, Melville, NY) mounted on a Zeiss Axioplan 2 microscope. Image calculations and measurements were performed with analySIS imaging software (Soft Imaging System, Münster, Germany).

A user-defined outline of each specimen was semiinteractively created and converted into a black-and-white mask. A gray-scale euclidian distance map was computed from the black-and-white mask and thresholds were applied, using seven gray-level ranges of equal width. Seven binary images were created in this way, serving as zone-delimiting masks in further analysis of the original digital image (Fig. 1a–f). Using this procedure, the user-defined outline of each specimen was automatically divided into seven consecutive concentric zones of approximately 500 μm. Zone 1 represents the outer 500 μm of a specimen, zone 2 the layer between 500 and 1000 μm, and so on. Zone 7 consists of the center of the specimen (Fig. 2).

To optimize color contrasts between ingrown tissue and polymer scaffold in the red–green–blue spectrum, adjustments were made in the hue–saturation–intensity spectrum of the original digital images (Fig. 1g). These adjustments were the same for all samples and were automatically applied to all images by the image analysis routine; no user input was required. In this way, polymer scaffold material that was stained blue by the Sudan black became bright red in the adjusted image, whereas ingrown tissue that was stained pink by the nuclear fast red became bright green in the adjusted image. Red–green–blue thresholds were then automatically applied to distinguish between scaffold material, tissue, and unfilled pores by color. A color-coded preview was then presented to the user to check the quality of the threshold settings and to allow for any minor adjustments. As the staining was homogeneous, similar threshold settings were used for all samples. Pixels representing tissue were counted and expressed as a percentage of the total number of pixels in each zone, resulting in an area percentage for each zone in each specimen (Fig. 1h and i, and Fig. 3).

Statistical analysis

Analysis of variance (ANOVA) were performed, one for each zone, testing for the main effects of postimplantation time and scaffold material on tissue ingrowth into the samples. An interaction factor between postimplantation time and scaffold material was added to the

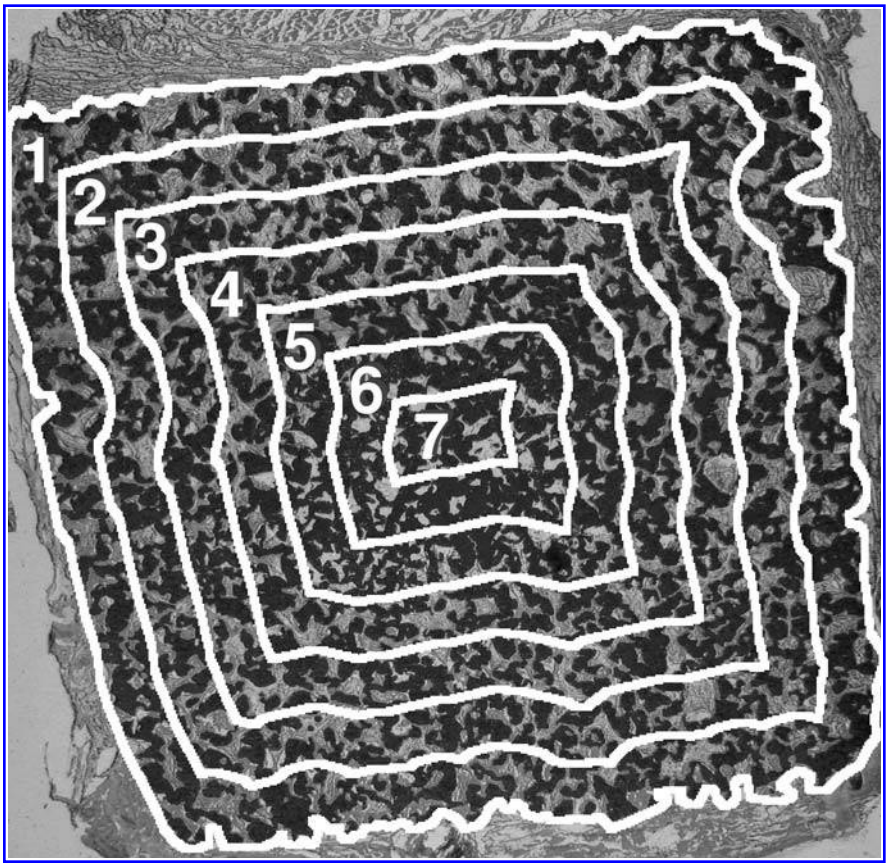

FIG. 2. Definition of seven concentric zones. All zones are of equal width.

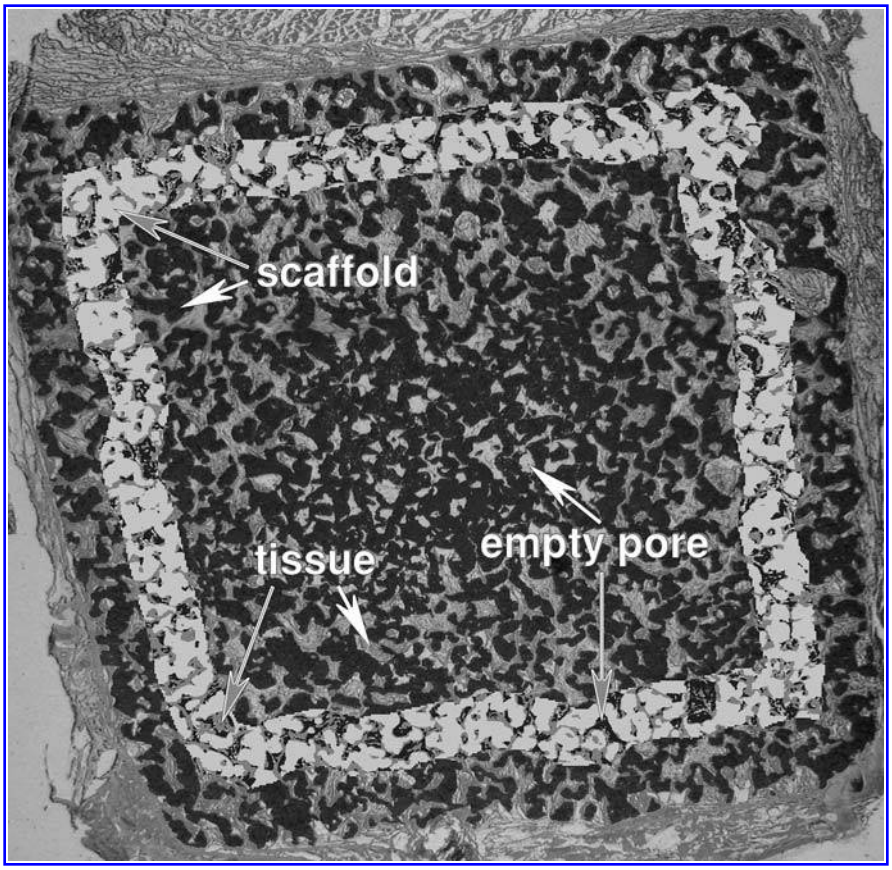

FIG. 3. In each zone (zone 2 in this case) the area percentage of ingrown tissue is determined. Tissue, scaffold, and empty pores are automatically color-coded during processing. Color-coding scheme: scaffold, white, empty pore, black; tissue, gray.

ANOVA model to enable testing for significant differences in tissue ingrowth rates. Post hoc Tukey tests were used to test for statistical significant differences in tissue ingrowth between the two polymers for corresponding zones at corresponding postimplantation time points ($\alpha = 0.05$). In addition, differences between zones were examined per scaffold material, using post hoc Tukey tests.

Between- and within-observer variability

To assess the between-observer and within-observer variation of the method employed, 16 randomly selected samples were measured by 2 independent observers. Within-observer variation was assessed by remeasuring samples for a second time by one of the observers (N.N.R.). Absolute differences were calculated. To assess whether the between-observer and within-observer variations were different for different zones, the correlation between the absolute difference and zone was determined.

In addition, to demonstrate that manual outlining of the samples hardly influenced measurement variability, samples were remeasured twice, using outlines of both observers but color threshold settings of only one observer.

RESULTS

Histology

Tissue growing into the scaffolds consisted mostly of fibrous tissue. Initially, at 1 week postimplantation, fields of fibrin matrix filled the pores of both Estane and PCLPU scaffolds. This matrix was first populated by scarce polymorphonuclear lymphocytes, followed by fibroblasts that increased in number with longer postimplantation times. At 4 weeks postimplantation the extracellular matrix had started to organize and showed more orientation. At 26 weeks postimplantation the remodeling of the matrix had progressed still further and all pores were completely filled with fibrous tissue.

Few blood vessels were seen 1 week postimplantation in contrast to 4 weeks postimplantation, at which time vascularization of mostly the periphery of the scaffolds had occurred. Ingrowth of tissue and vessels progressed with later postimplantation times. Along with the vascularization, more polymorphonuclear lymphocytes could be found in both scaffold types. Also, a steady increase in the number of foreign body giant cells was observed over time on the surface of both scaffold types. In par-

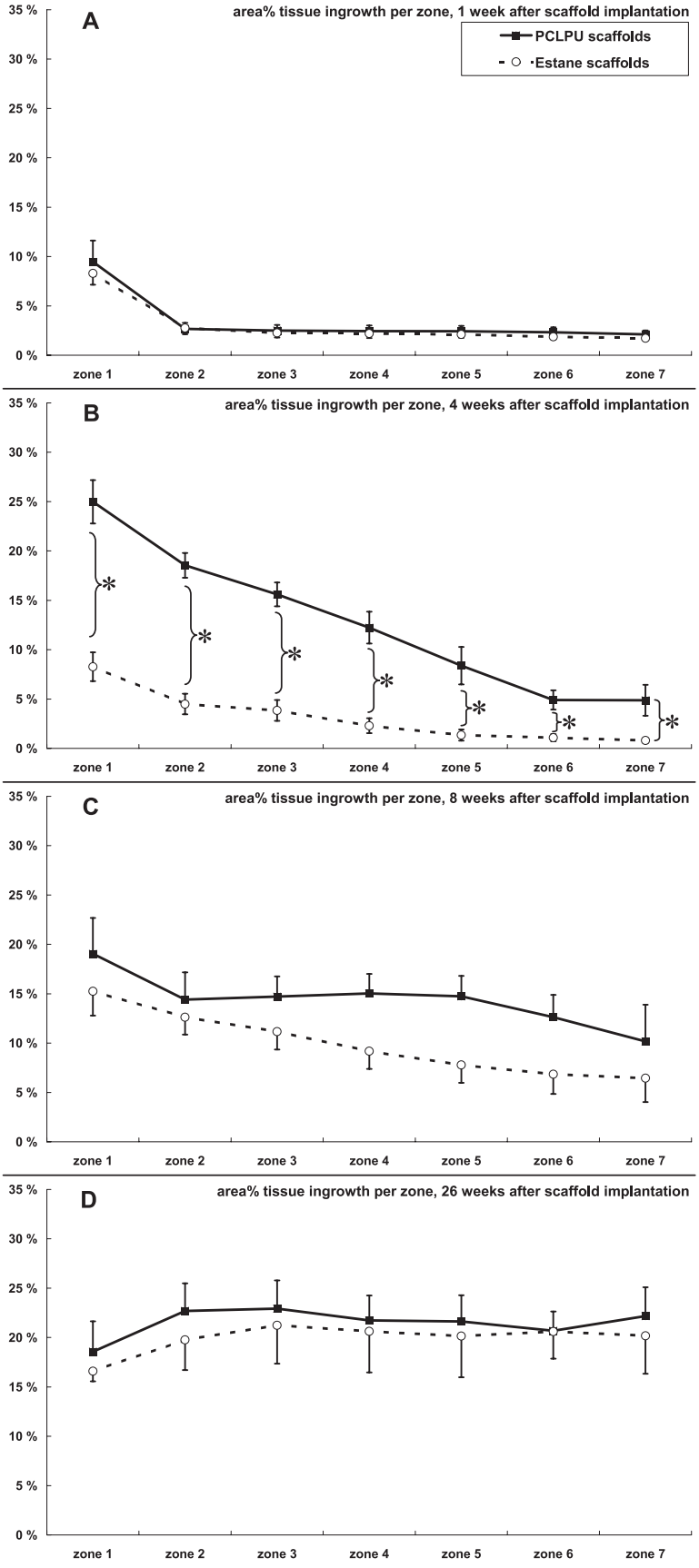

FIG. 4. Area percentage of tissue ingrowth per zone at 1 week (**A**), 4 weeks (**B**), 8 weeks (**C**), and 26 weeks (**D**) postimplantation. Error bars represent standard errors of the mean. An asterisk indicates a significant difference between PCLPU and Estane scaffolds.

ticular, Estane scaffolds 24 weeks postimplantation showed clusters of macrophages with a brown content. This was not observed in PCLPU scaffolds. No morphological changes indicating scaffold degradation were found in either scaffold.

Histomorphometry

Especially at earlier postimplantation times, pores located deep within both scaffold types remained empty, whereas superficial pores already contained some tissue (Fig. 3). Correspondingly, this can be observed most clearly in Fig. 4A, where the lines representing 1 week postoperation show a clear step-off between the superficial zone 1 and deeper zones. For both scaffold materials, ingrowth into the first zone was significantly different from ingrowth into the second and deeper zones.

In addition, progression of ingrown tissue from the surface of the scaffold toward the center was observed over time. At increasing postimplantation time points more tissue ingrowth was seen and in deeper zones (Figure 4A–D). At 4 weeks postimplantation (Fig. 4B) both lines show a decline, indicating the presence of a tissue ingrowth gradient. This can also be observed in Figs. 5 and 6. At 8 weeks postimplantation (Fig. 4C) the same feature can be observed, although to a lesser extent; the decline is less evident. At 26 weeks, deep and superficial zones show similar area percentages of tissue ingrowth (differences between zones are not statistically significant), resulting in relatively horizontal lines (Fig. 4D).

Not only does Fig. 4 show that tissue ingrowth progresses with increasing postimplantation time, but it also shows that at later postimplantation times tissue ingrowth continues in zones that were among the first to be invaded by tissue; the area percentage of tissue ingrowth per zone tends to be higher at later postimplantation periods, even in the outer zones. This further illustrates the fact that indeed there is a tissue ingrowth gradient rather than a tissue ingrowth front.

Statistical analysis

ANOVA testing for the main effects of postimplantation time (1, 4, 8, and 26 weeks) and scaffold material on tissue ingrowth showed that there was a significant difference in ingrowth between the polymers for all zones (Table 2). When postimplantation time points were considered separately, post hoc testing showed significant differences between PCLPU scaffolds and Estane scaffolds at 4 weeks post-implantation (Fig. 4B). In all zones, the polycaprolactone–polyurethane scaffolds showed significantly more tissue ingrowth than Estane. No significant differences were found at 1, 8, and 26 weeks postimplantation.

In the ANOVA, the interaction factor between postimplantation time and scaffold material was statistically significant for zones 1 through 3 only, indicating significantly different ingrowth rates between PCLPU and Estane in zones 1 through 3, considering postimplantation times of 1, 4, 8, and 26 weeks (Table 1).

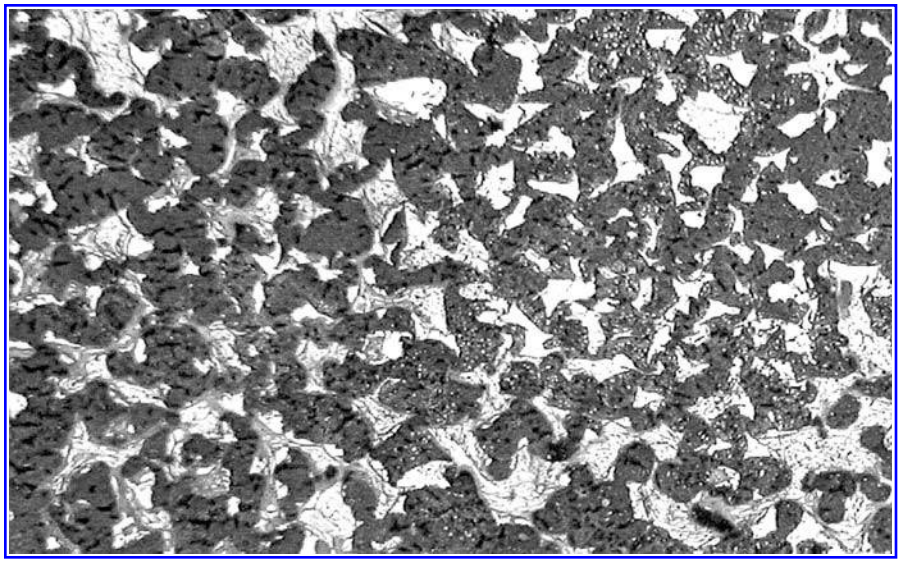

FIG. 5. Detailed view of a tissue ingrowth gradient, showing the progressive location of tissue within pores. In the upper right-hand corner, pores hardly contain any tissue, not even along the pore edges. In the lower left-hand corner, pores contain much more tissue, although the pores are not completely filled yet. Tissue is situated both along the edge of pores but also in the middle of pores. In the upper left-hand corner, center, and lower right-hand corner tissue is situated mostly along the edge of pores and hardly in the middle of pores.

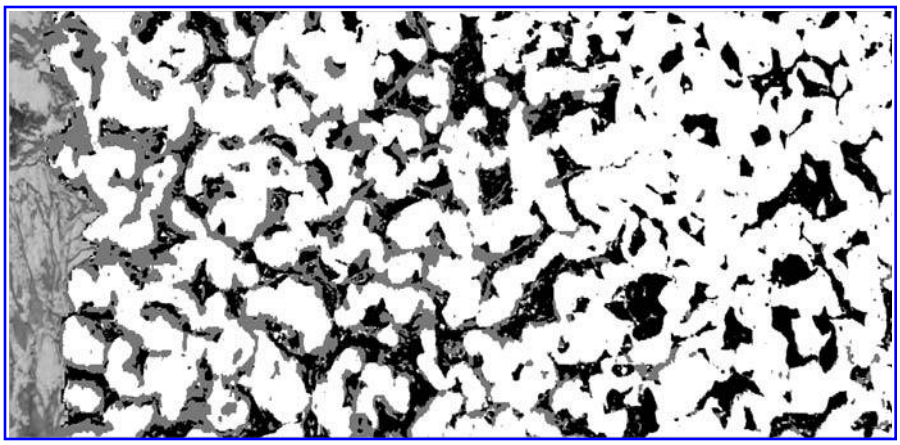

FIG. 6. Detailed view of a color-coded image illustrating the presence of a tissue ingrowth gradient rather than a clearly defined tissue ingrowth front. Pores (black) in the polymer (white) are usually partially filled with tissue (gray). On the left-hand side (superficial) pores contain more tissue than on the right-hand side (deep). A clear cutoff cannot be defined.

Because ingrowth at 26 weeks was complete for both polymers, 26-week data were noninformative to determine ingrowth rates. The ANOVA that excluded 26-week data showed that ingrowth rates of PCLPU and Estane were significantly different for zones 1 through 6 (Table 2).

Between-observer and within-observer differences are presented in Table 3. There was no statistically significant correlation between absolute difference and zone. Drawing the outlines a second time by the same observer caused a mean absolute difference of 0.26% (SEM, 0.058%; 5th percentile, 0.0029%; 95th percentile difference, 1.1%).

DISCUSSION

This study employs a simple method to assess tissue ingrowth into a porous biomaterial, resulting in detailed quantitative information that can be interpreted easily. The process is highly automated, reducing the possibility for human error, interobserver differences, and time spent on data acquisition. Limitations to this method are similar to those of any other histomorphometric analysis, as tissue and biomaterial need to be distinguishable by color. To the authors' knowledge, no reports exist in current literature employing the same method for assessment of tissue ingrowth. Although numerous other histomorphometric studies measure ingrowth distance unidirectionally and measure ingrowth area,[34] we account for multidirectionality of ingrowth by using ingrowth zones, which has not been done previously in large scaffolds. Theoretically, small differences in ingrowth rate will be detected more reliably using ingrowth zones as compared with histomorphometric methods that measure the overall ingrowth area in an entire sample.

Other histomorphometric methods[27] often attempt to define a tissue ingrowth front, assuming that tissue in-

TABLE 1. *p* VALUES IN ANOVA OF DIFFERENCES IN INGROWTH BETWEEN PCLPU AND ESTANE ACROSS ALL POST IMPLANTATION TIME POINTS

Zone	p *Values of difference in tissue ingrowth between PCLPU and Estane*	p *Values of difference in tissue ingrowth rates between PCLPU and Estane (interaction between time and material)*
1	0.002	0.009
2	<0.0005	0.004
3	<0.0005	0.017
4	<0.0005	0.063[a]
5	<0.0005	0.099[a]
6	<0.0005	0.083[a]
7	<0.0005	0.436[a]

Abbreviations: ANOVA, analysis of variance; PCLPU, polycaprolactone–polyurethane.
[a]Not significant.

Table 2. *p* Values in ANOVA of Differences in Ingrowth between PCLPU and Estane across All Post Implantation Time Points, Excluding 26 Weeks Postimplantation

Zone	p *Values of difference in tissue ingrowth between PCLPU and Estane*	p *Values of difference in tissue ingrowth rates between PCLPU and Estane (interaction between time and material)*
1	0.001	0.005
2	0.001	0.001
3	<0.0005	0.003
4	0.001	0.017
5	0.001	0.046
6	0.012	0.028
7	0.013	0.26[a]

[a]Not significant.

growth is a dichotomous variable; either a pore is filled with tissue or it is not. Most of the time, this is not the case as the filling of a series of neighboring pores coincides, although be it with a slight delay, rather than filling up consecutively (Figs. 4 and 5). A tissue ingrowth front may therefore be difficult to define when there actually is a tissue ingrowth gradient. User intervention is usually required in these cases. The histomorphometric method proposed in this study will simply show a gradient when there is one, without taking any extra time or effort.

In this study, a user-defined outline was created semi-interactively by defining the corners of a polygon on the digitized midsections of the scaffold samples. An automated edge detection routine optimized for these samples could have been devised for this task. Alhough perhaps more time efficient, it is unlikely that such a routine would have decreased observer variability, as the outline procedure contributed only approximately 1% to the variability. Other studies using different samples may benefit from such a edge detection routine, however. Furthermore, we showed that measurement variation was independent of zone. This emphasizes that the measurement variation will not have caused an underestimation or overestimation of tissue ingrowth rate. If the measurement variation were dependent on zone, this could have led to wrong conclusions regarding the ingrowth pattern. Thus, subdivision in zones does not entail any extra risks of making false inferences on ingrowth rates.

Even though in this study much effort was made to preserve observer independence, some observer dependence inevitably remains. Optimization of color thresholds used by the image analysis routine to distinguish between tissue, scaffold, and unfilled pores was done interactively within constraints. As indicated by our results of between- and within-observer variability, variability stemmed predominantly from the optimization of these settings. This difficulty is inherent to all histomorphometric analyses, however, and the authors do not presume this study to be exempt from those limitations. Nevertheless, in comparison with the frequently used method that depends on the experience of the user in discerning where exactly a tissue ingrowth front is located, the proposed method in this study effectively eliminates that substantial source of both inter- and intraobserver variability. Especially in samples where there is a tissue ingrowth gradient, as is often the case, the proposed method could prove to be superior.

PCLPU scaffolds showed ingrowth rates higher than those in Estane scaffolds. This is best reflected in the 4-week postimplantation results, where a marked difference in both amount and depth of tissue infiltration was ob-

Table 3. Between-Observer and Within-Observer Variation Expressed as Absolute Differences in Tissue Ingrowth Area Percentage[a]

	Between-observer difference (%)	*Within-observer difference (%)*
Mean ± SEM	2.6 ± 0.3	2.0 ± 0.2
5th percentile	0.06	0.10
95th percentile	10.8	5.2

[a]Measurements are percentages and therefore absolute differences are expressed as percentages as well.

served. Later on, at 26 weeks postimplantation, both scaffold materials were fully infiltrated by tissue already and differences in ingrowth rates obviously could no longer be assessed. Most likely, however, tissue ingrowth into PCLPU scaffolds was completed no later than in Estane scaffolds.

In this study, no morphological changes indicating degradation of scaffolds were found after 26 weeks postimplantation. Indeed, it is unlikely that such changes could have been observed microscopically at this follow-up time. A long-term *in vitro* degradation study of PCLPU scaffolds showed that even though after 9 months the deterioration of biomechanical properties of the scaffolds was significant, no signs of degradation could be found by scanning electron microscopy.[35]

Estane scaffolds and PCLPU scaffolds had identical permeability, in terms of porosity and pore size, and compression modulus. These scaffold properties are essential for tissue ingrowth and differentiation into fibrocartilage when scaffolds are used for meniscus tissue engineering.[36,37] However, two scaffolds manufactured from different materials but with identical porosity, pore size, and compression modulus do not necessarily demonstrate equal tissue ingrowth rates as chemical and physical properties can signifincatly influence biocompatibility. It therefore remains necessary to test new scaffolds for their capacity to allow tissue ingrowth and proliferation as results from other scaffolds cannot be extrapolated automatically. For instance, Estane and PCLPU scaffolds may have had quite different levels of phase separation between hard and soft segments. This phenomenon results in disproportionate amounts of either hard or soft segment being exposed at the surface of the polymer, shielding the other segment from the scaffold–tissue interface.[38] Hard and soft segments differ in hydrophilicity. It is well known that the level of hydrophilicity of a polymer surface plays an important role in cell adhesion and proliferation[39] and thus quite likely will affect tissue ingrowth. However, differences herein can be mitigated *in vivo* when protein-rich extracellular fluids (e.g., blood) settle down onto the scaffold surface and mediate between the cells and polymer.

To what extent can the results of our subcutaneous implantation model be extrapolated to meniscus tissue engineering, since the characteristics of the surrounding tissue in this study differ from the characteristics of meniscus tissue? We believe that subcutaneous implantation of scaffolds can be used to screen polymers as possible candidates for meniscus implantation studies. A polymer that presents poor ingrowth at a subcutaneous implantation site is unlikely to show better ingrowth in a less favorable environment such as the knee. Indeed, data on tissue ingrowth in Estane scaffolds that were implanted in dog knees showed that tissue ingrowth in this environment is good.[40] Fibrovascular tissue ingrowth into 3.5-mm-wide Estane meniscus prostheses was complete 3 months postimplantation.[40] Because tissue ingrowth for subcutaneous implanted Estane scaffolds in the present study was also good, and for PCLPU even better than for Estane, the nontoxic PCLPU scaffold[30,31] is a serious candidate for an animal study investigating meniscus implantation. However, the ultimate goal is to achieve differentiation of ingrown tissue toward fibrocartilage. In fact, such was observed in the same study. Six months postimplantation in dogs, fibrocartilage-like tissue was found in the Estane meniscus prostheses.[40] Unfortunately, as previously mentioned, Estane is thought to have toxic degradation products in the long term.[29] Whether tissue in a PCLPU meniscus prosthesis will show similar differentiation into fibrocartilage-like tissue remains to be seen.

In conclusion, this study demonstrates a novel, sensitive, histomorphometric method to assess tissue ingrowth into porous polymer scaffolds. This method may prove to be particularly useful when rates of tissue ingrowth are being investigated in the field of biomaterial development or modulation of tissue ingrowth by growth factors.

ACKNOWLEDGMENTS

The authors gratefully acknowledge Natasja Lieuwes and Leon Driessen for excellent technical assistance. Funding for this research was provided by the Netherlands Technology Foundation (NWO/STW 349-4771).

REFERENCES

1. Vacanti, C.A., Langer, R., Schloo, B., and Vacanti, J.P. Synthetic polymers seeded with chondrocytes provide a template for new cartilage formation. Plast. Reconstr. Surg. **88,** 753, 1991.
2. Grad, S., Kupcsik, L., Gorna, K., Gogolewski, S., and Alini, M. The use of biodegradable polyurethane scaffolds for cartilage tissue engineering: Potential and limitations. Biomaterials **24,** 5163, 2003.
3. Buma, P., Pieper, J.S., van Tienen, T., van Susante, J.L., van der Kraan, P.M., Veerkamp, J.H., van den Berg, W.B., Veth, R.P., and van Kuppevelt, T.H. Cross-linked type I and type II collagenous matrices for the repair of full-thickness articular cartilage defects: A study in rabbits. Biomaterials **24,** 3255, 2003.
4. Hutmacher, D.W., Ng, K.W., Kaps, C., Sittinger, M., and Klaring, S. Elastic cartilage engineering using novel scaffold architectures in combination with a biomimetic cell carrier. Biomaterials **24,** 4445, 2003.
5. Frenkel, S.R., and Di Cesare, P.E. Scaffolds for articular cartilage repair. Ann. Biomed. Eng. **32,** 26, 2004.
6. Harris, C.T., and Cooper, L.F. Comparison of bone graft matrices for human mesenchymal stem cell-directed osteogenesis. J. Biomed. Mater. Res. **68A,** 747, 2004.

7. Sharma, B., and Elisseeff, J.H. Engineering structurally organized cartilage and bone tissues. Ann. Biomed. Eng. **32,** 148, 2004.
8. Warren, S.M., Nacamuli, R.K., Song, H.M., and Longaker, M.T. Tissue-engineered bone using mesenchymal stem cells and a biodegradable scaffold. J. Craniofac. Surg. **15,** 34, 2004.
9. Buma, P., Schreurs, W., and Verdonschot, N. Skeletal tissue engineering. From *in vitro* studies to large animal models. Biomaterials **25,** 1487, 2004.
10. Risbud, M.V., Karamuk, E., Schlosser, V., and Mayer, J. Hydrogel-coated textile scaffolds as candidate in liver tissue engineering. II. Evaluation of spheroid formation and viability of hepatocytes. J. Biomater. Sci. Polym. Ed. **14,** 719, 2003.
11. Barralet, J.E., Wallace, L.L., and Strain, A.J. Tissue engineering of human biliary epithelial cells on polyglycolic acid/polycaprolactone scaffolds maintains long-term phenotypic stability. Tissue Eng. **9,** 1037, 2003.
12. Xu, C.Y., Inai, R., Kotaki, M., and Ramakrishna, S. Aligned biodegradable nanofibrous structure: A potential scaffold for blood vessel engineering. Biomaterials **25,** 877, 2004.
13. Harding, S.I., Afoke, A., Brown, R.A., MacLeod, A., Shamlou, P.A., and Dunnill, P. Engineering and cell attachment properties of human fibronectin–fibrinogen scaffolds for use in tissue engineered blood vessels. Bioprocess. Biosyst. Eng. **25,** 53, 2002.
14. He, H., and Matsuda, T. Arterial replacement with compliant hierarchic hybrid vascular graft: Biomechanical adaptation and failure. Tissue Eng. **8,** 213, 2002.
15. Rothenburger, M., Volker, W., Vischer, J.P., Berendes, E., Glasmacher, B., Scheld, H.H., and Deiwick, M. Tissue engineering of heart valves: Formation of a three-dimensional tissue using porcine heart valve cells. ASAIO J. **48,** 586, 2002.
16. Kim, W.G., Cho, S.K., Kang, M.C., Lee, T.Y., and Park, J.K. Tissue-engineered heart valve leaflets: An animal study. Int. J. Artif. Organs **24,** 642, 2001.
17. Buma, P., Ramrattan, N.N., van Tienen, T.G., and Veth, R.P. Tissue engineering of the meniscus. Biomaterials **25,** 1523, 2004.
18. De Groot, J.H., de Vrijer, R., Pennings, A.J., Klompmaker, J., Veth, R.P., and Jansen, H.W. Use of porous polyurethanes for meniscal reconstruction and meniscal prostheses. Biomaterials **17,** 163, 1996.
19. Tienen, T.G., Heijkants, R.G., Buma, P., De Groot, J.H., Pennings, A.J., and Veth, R.P. A porous polymer scaffold for meniscal lesion repair. A study in dogs. Biomaterials **24,** 2541, 2003.
20. Flanagan, T.C., and Pandit, A. Living artificial heart valve alternatives: A review. Eur. Cell Mater. **6,** 28, 2003.
21. Kim, S.S., Utsunomiya, H., Koski, J.A., Wu, B.M., Cima, M.J., Sohn, J., Mukai, K., Griffith, L.G., and Vacanti, J.P. Survival and function of hepatocytes on a novel three-dimensional synthetic biodegradable polymer scaffold with an intrinsic network of channels. Ann. Surg. **228,** 8, 1998.
22. Fuchs, J.R., Pomerantseva, I., Ochoa, E.R., Vacanti, J.P., and Fauza, D.O. Fetal tissue engineering: *In vitro* analysis of muscle constructs. J. Pediatr. Surg. **38,** 1348, 2003.
23. Horner, H.A., and Urban, J.P. 2001 Volvo Award Winner in Basic Science Studies: Effect of nutrient supply on the viability of cells from the nucleus pulposus of the intervertebral disc. Spine **26,** 2543, 2001.
24. Lutolf, M.P., Weber, F.E., Schmoekel, H.G., Schense, J.C., Kohler, T., Muller, R., and Hubbell, J.A. Repair of bone defects using synthetic mimetics of collagenous extracellular matrices. Nat. Biotechnol. **21,** 513, 2003.
25. Tabata, Y., Miyao, M., Yamamoto, M., and Ikada, Y. Vascularization into a porous sponge by sustained release of basic fibroblast growth factor. J. Biomater. Sci. Polym. Ed. **10,** 957, 1999.
26. Saito, N., and Takaoka, K. New synthetic biodegradable polymers as BMP carriers for bone tissue engineering. Biomaterials **24,** 2287, 2003.
27. Yamamoto, M., Tabata, Y., Kawasaki, H., and Ikada, Y. Promotion of fibrovascular tissue ingrowth into porous sponges by basic fibroblast growth factor. J. Mater. Sci. Mater. Med. **11,** 213, 2000.
28. Wake, M.C., Mikos, A.G., Sarakinos, G., Vacanti, J.P., and Langer, R. Dynamics of fibrovascular tissue ingrowth in hydrogel foams. Cell Transplant. **4,** 275, 1995.
29. Szycher, M. Biostability of polyurethane elastomers: A critical review. J. Biomater. Appl. **3,** 297, 1988.
30. Pitt, C.G. In: Chasin, M., and Langer, R., eds. Biodegradable Polymers as Drug Delivery Systems. New York: Marcel Dekker, 1990, pp. 71–120.
31. Bogdanov, B., Toncheva, V., Schacht, E., Finelli, L., Sarti, B., and Scandola, M. Physical properties of poly(ester-urethanes) prepared from different molar mass polycaprolactone-diols. Polymer **40,** 3171, 1999.
32. Degroot, J.H., Nijenhuis, A.J., Bruin, P., Pennings, A.J., Veth, R.P.H., Klompmaker, J., and Jansen, H.W.B. Use of porous biodegradable polymer implants in meniscus reconstruction. 1. Preparation of porous biodegradable polyurethanes for the reconstruction of meniscus lesions. Colloid Polym. Sci. **268,** 1073, 1990.
33. Heijkants, R.G.J.C., van Calck, R.V., De Groot, J.H., Pennings, A.J., Schouten, A.J., van Tienen, T.G., Ramrattan, N., Buma, P., and Veth, R.P.H. Design, synthesis and properties of a degradable polyurethane scaffold for meniscus regeneration. J. Mater. Sci. Mater. Med. **15,** 423, 2004.
34. Huffer, W.E., Ruegg, P., Zhu, J.M., and Lepoff, R.B. Semi-automated methods for cancellous bone histomorphometry using a general-purpose video image analysis system. J. Microsc. **173,** 53, 1994.
35. Heijkants, R.G.J.C. Polyurethane scaffolds as meniscus reconstruction materials [Ph.D. thesis]. Department of Polymer Chemistry, University of Groningen, Groningen, The Netherlands, 2004.
36. Klompmaker, J., Jansen, H.W.B., Veth, R.P.H., Nielsen, H.K.L., de Groot, J.H., and Pennings, A.J. Porous implants for knee joint meniscus reconstruction: A preliminary study on the role of pore sizes in ingrowth and differentiation of fibrocartilage. Clin. Mater. **14,** 1, 1993.
37. van Tienen, T.G., Heijkants, R.G.J.C., Buma, P., de Groot, J.H., Pennings, A.J., and Veth, R.P.H. Tissue ingrowth and degradation of two biodegradable porous polymers with different porosities and poresizes. Biomaterials **23,** 1731, 2002.

38. Lambda N.M.K., Woodhouse, K.A., and Cooper, S.L., eds. Surface characterization of polyurethanes. In: Polyurethanes in Biomedical Applications. Boca Raton, FL: CRC Press, 1998, p. 91.
39. Lee, J. H., and Lee, H.B. A wettability gradient as a tool to study protein adsorption and cell adhesion on polymer surfaces. J. Biomater. Sci. Polym. Ed. **4,** 467, 1993.
40. van Tienen, T.G. *in vivo* tissue engineering of the knee joint meniscus [Ph.D. thesis]. Department of Orthopedics. Universty Medical Center St. Radboud, Nijmegen, The Netherlands, 2004.

Address reprint requests to:
Navin N. Ramrattan, MD
Spank 72
4824 BG Breda, The Netherlands

E-mail: n_ramrattan@yahoo.com

This article has been cited by:

1. Gerjon Hannink, Eric L.W. de Mulder, Tony G. van Tienen, Pieter Buma. 2012. Effect of load on the repair of osteochondral defects using a porous polymer scaffold. *Journal of Biomedical Materials Research Part B: Applied Biomaterials* **100B**:8, 2082-2089. [CrossRef]
2. Han Su Kim, Sung Min Chung, Soo Yeon Jung, Soo Jin Kim, Kyung Yeon Kim. 2012. Porous Polyurethane Scaffold as a Tracheal Prosthesis Material. *Korean Journal of Otorhinolaryngology-Head and Neck Surgery* **55**:1, 30. [CrossRef]
3. Eleftherios A. Makris, Pasha Hadidi, Kyriacos A. Athanasiou. 2011. The knee meniscus: Structure–function, pathophysiology, current repair techniques, and prospects for regeneration. *Biomaterials* **32**:30, 7411-7431. [CrossRef]
4. Natalie K. Galley, Jason P. Gleghorn, Scott Rodeo, Russell F. Warren, Suzanne A. Maher, Lawrence J. Bonassar. 2011. Frictional Properties of the Meniscus Improve After Scaffold-augmented Repair of Partial Meniscectomy: A Pilot Study. *Clinical Orthopaedics and Related Research®* . [CrossRef]
5. Lara C. Ionescu , Gregory C. Lee , Grant H. Garcia , Tiffany L. Zachry , Roshan P. Shah , Brian J. Sennett , Robert L. Mauck . 2011. Maturation State-Dependent Alterations in Meniscus Integration: Implications for Scaffold Design and Tissue Engineering. *Tissue Engineering Part A* **17**:1-2, 193-204. [Abstract] [Full Text HTML] [Full Text PDF] [Full Text PDF with Links]
6. Jorn Op Den Buijs , Erik L. Ritman , Dan Dragomir-Daescu . 2010. Validation of a Fluid–Structure Interaction Model of Solute Transport in Pores of Cyclically Deformed Tissue Scaffolds. *Tissue Engineering Part C: Methods* **16**:5, 1145-1156. [Abstract] [Full Text HTML] [Full Text PDF] [Full Text PDF with Links]
7. T. CHANDYBiocompatibility of materials and its relevance to drug delivery and tissue engineering 301-325. [CrossRef]
8. Stephanie Grenier , Martin Sandig , Kibret Mequanint . 2009. Smooth Muscle #-Actin and Calponin Expression and Extracellular Matrix Production of Human Coronary Artery Smooth Muscle Cells in 3D Scaffolds. *Tissue Engineering Part A* **15**:10, 3001-3011. [Abstract] [Full Text HTML] [Full Text PDF] [Full Text PDF with Links]
9. Christopher Moraes, Yoan K. Kagoma, Bogdan M. Beca, Rachel L.M. Tonelli-Zasarsky, Yu Sun, Craig A. Simmons. 2009. Integrating polyurethane culture substrates into poly(dimethylsiloxane) microdevices. *Biomaterials* **30**:28, 5241-5250. [CrossRef]
10. Jorn Op Den Buijs , Lichun Lu , Steven M. Jorgensen , Dan Dragomir-Daescu , Michael J. Yaszemski , Erik L. Ritman . 2009. Solute Transport in Cyclically Deformed Porous Tissue Scaffolds with Controlled Pore Cross-Sectional Geometries. *Tissue Engineering Part A* **15**:8, 1989-1999. [Abstract] [Full Text HTML] [Full Text PDF] [Full Text PDF with Links]
11. Yuen Kee Tsui, Sylwester Gogolewski. 2009. Microporous biodegradable polyurethane membranes for tissue engineering. *Journal of Materials Science: Materials in Medicine* **20**:8, 1729-1741. [CrossRef]
12. B. G. Sengers, C. P. Please, M. Taylor, R. O. C. Oreffo. 2009. Experimental–Computational Evaluation of Human Bone Marrow Stromal Cell Spreading on Trabecular Bone Structures. *Annals of Biomedical Engineering* **37**:6, 1165-1176. [CrossRef]
13. Jonathan D. Packer, Scott A. Rodeo. 2009. Meniscal Allograft Transplantation. *Clinics in Sports Medicine* **28**:2, 259-283. [CrossRef]
14. Masahiro Kino-Oka, Yasunori Takezawa, Masahito Taya. 2009. Quality control of cultured tissues requires tools for quantitative analyses of heterogeneous features developed in manufacturing process. *Cell and Tissue Banking* **10**:1, 63-74. [CrossRef]
15. Ji Sun Park, Dae Gyun Woo, Han Na Yang, Hye Jin Lim, Kyong Mi Park, Kun Na, Keun-Hong Park. 2009. Chondrogenesis of human mesenchymal stem cells encapsulated in a hydrogel construct: Neocartilage formation in animal models as both mice and rabbits. *Journal of Biomedical Materials Research Part A* **9999A**, NA-NA. [CrossRef]
16. R. G. J. C. Heijkants, R. V. van Calck, T. G. van Tienen, J. H. de Groot, A. J. Pennings, P. Buma, R. P. H. Veth, A. J. Schouten. 2008. Polyurethane scaffold formation via a combination of salt leaching and thermally induced phase separation. *Journal of Biomedical Materials Research Part A* **87A**:4, 921-932. [CrossRef]
17. Hong-Shik Choi, Hwal Suh, Ja-Hyun Lee, Si-Nae Park, Sang-Hyun Shin, Young-Ho Kim, Sung Min Chung, Hyun Kyung Kim, Jae-Yol Lim, Han Su Kim. 2008. A polyethylene glycol grafted bi-layered polyurethane scaffold: preliminary study of a new candidate prosthesis for repair of a partial tracheal defect. *European Archives of Oto-Rhino-Laryngology* **265**:7, 809-816. [CrossRef]
18. Keun Hong Park, Kun Na. 2008. Effect of growth factors on chondrogenic differentiation of rabbit mesenchymal cells embedded in injectable hydrogels. *Journal of Bioscience and Bioengineering* **106**:1, 74-79. [CrossRef]

19. Masahiro Kino-oka, Yoshikatsu Maeda, Yasuaki Sato, Ali Baradar Khoshfetrat, Takeyuki Yamamoto, Katsura Sugawara, Masahito Taya. 2008. Characterization of spatial growth and distribution of chondrocyte cells embedded in collagen gels through a stereoscopic cell imaging system. *Biotechnology and Bioengineering* **99**:5, 1230-1240. [CrossRef]
20. Kyusik Yun, Hyun Tae Moon. 2008. Inducing Chondrogenic Differentiation in Injectable Hydrogels Embedded with Rabbit Chondrocytes and Growth Factor for Neocartilage Formation. *Journal of Bioscience and Bioengineering* **105**:2, 122-126. [CrossRef]
21. Greg Lemon, Sarah L. Waters, Felicity R.A.J. Rose, John R. King. 2007. Mathematical modelling of human mesenchymal stem cell proliferation and differentiation inside artificial porous scaffolds. *Journal of Theoretical Biology* **249**:3, 543-553. [CrossRef]
22. G. Lemon, J. R. King. 2007. Travelling-wave behaviour in a multiphase model of a population of cells in an artificial scaffold. *Journal of Mathematical Biology* **55**:4, 449-480. [CrossRef]
23. Andre F. Steinert , Glyn D. Palmer , Ramille Capito , Jochen G. Hofstaetter , Carmencita Pilapil , Steven C. Ghivizzani , Myron Spector , Christopher H. Evans . 2007. Genetically Enhanced Engineering of Meniscus Tissue Using Ex Vivo Delivery of Transforming Growth Factor-#1 Complementary Deoxyribonucleic Acid. *Tissue Engineering* **13**:9, 2227-2237. [Abstract] [Full Text PDF] [Full Text PDF with Links]
24. Joseph Jagur-Grodzinski. 2006. Polymers for tissue engineering, medical devices, and regenerative medicine. Concise general review of recent studies. *Polymers for Advanced Technologies* **17**:6, 395-418. [CrossRef]
25. Chapter 3 Basic Technologies Developed for Tissue Engineering **8**, 235-421. [CrossRef]